VIP Microfiber Arrays Very Important Paper

How to cite:
International Edition: doi.org/10.1002/anie.202102833
German Edition: doi.org/10.1002/ange.202102833

Long-Term Tracking and Dynamically Quantifying of Reversible Changes of Extracellular Ca^{2+} in Multiple Brain Regions of Freely Moving Animals

*Yuandong Liu, Zhichao Liu, Fan Zhao, and Yang Tian**

Abstract: *Understanding physiological and pathological processes in the brain requires tracking the reversible changes in chemical signals with long-term stability. We developed a new anti-biofouling microfiber array to real-time quantify extracellular Ca^{2+} concentrations together with neuron activity across many regions in the mammalian brain for 60 days, in which the signal degradation was < ca. 8 %. The microarray with high tempo-spatial resolution (ca. 10 μm, ca. 1.3 s) was implanted into 7 brain regions of free-moving mice to monitor reversible changes of extracellular Ca^{2+} upon ischemia-reperfusion processes. The changing sequence and rate of Ca^{2+} in 7 brain regions were different during the stroke. ROS scavenger could protect Ca^{2+} influx and neuronal activity after stroke, suggesting the significant influence of ROS on Ca^{2+} overload and neuron death. We demonstrated this microarray is a versatile tool for investigating brain dynamic during pathological processes and drug treatment.*

Introduction

Monitoring neuronal signaling with chemical expression involved long-term physiological and pathological changes in vivo holds the key to dissecting the complex mechanisms of pathogenesis and drug treatment of brain diseases in behaving animals.[1] Although technologies such as electrophysiology[2] and non-invasive functional magnetic resonance imaging[3] have made significant progress in real-time monitoring of brain nerves, the methods for long-term monitoring of chemical species in vivo are still limited. Positron emission tomography, which maps the target molecules by injected probes, has recently been developed in freely moving mice by point source tracking.[4] However, it suffers from low spatial resolution. The electrochemical method provides a practical approach for monitoring chemical signals in vivo, in which the implanted functional microelectrode shows excellent tempo-spatial resolution.[5] Our group has designed a double-recognition strategy and developed a series of selectively electrochemical sensors to accurately monitor chemical species such as reactive oxygen species (ROS), amino acids, oxygen and pH, metal ion, and sulfide hydrogen in the brain.[6] More recently, we have designed and synthesized a novel molecule for specific recognition of Fe^{2+}, and assembled it onto the electrode surface through an Au–C≡C bond with high stability.[7] Although the developed methods are selective and accurate for detection in vivo, the recognition processes are usually irreversible. Thus, these methods are difficult for real-time tracking the dynamic changes of chemical species in the brain of behaving animals. Furthermore, it is still a challenge for long-term monitoring of chemical signals in the intricate brain, because many proteins existing in the brain are easy to adsorb onto the surfaces of implanted biosensors, resulting in signals loss.[8] Over the past decades, a lot of hydrophilic materials[9] have been developed to resist protein adsorption, based on the repulsive effect between the hydration layers of proteins and hydrophilic materials. Unfortunately, the surfaces completely protected by anti-biofouling materials are hard to modify the functional recognition molecules on the active sites of electrodes.

Here, to solve the above problems, we designed and developed a new type of anti-biofouling microfiber array for real-time tracking of extracellular Ca^{2+} changes with high reversibility and selectivity. The carbon fiber microelectrode (CFME) modified with gold particles was electrodeposited and alternately wrapped with graphene oxide microbands (GOMs), in which the exposed gold particles provided active sites for modification of recognition molecules. The developed electrode showed long-term stability for monitoring the chemical signals of Ca^{2+} in the brain of freely moving mice because of its remarkable anti-fouling property. The sensitivity of the present electrode was found to maintain ca. 92 % after this sensor was implanted and continuously measured in the live brain for 60 days. On the other hand, three kinds of Ca^{2+} ligands (METH, M18C6, and MBAPTA) with different recognition affinities were designed and assembled onto the developed microelectrodes. It was found that METH demonstrated the best reversibility and selectivity for determination of Ca^{2+}, among the synthesized three ligands. Eventually, 7 microelectrodes were constructed into a microfiber array for, respectively implanting into 7 brain regions of mice and monitoring the reversible changes of extracellular Ca^{2+} upon cerebral ischemia-reperfusion (I/R) processes (Figure 1 a). Meanwhile, because open-circuit potentiometry without any applied potentials or currents was employed in electrochemical measurements, a nickel-titanium wire electrode was used to record local field potential (LFP) simultaneously. Benefiting from the good reversibility and selectivity

[*] Y. Liu, Dr. Z. Liu, Dr. F. Zhao, Prof. Y. Tian
Shanghai Key Laboratory of Green Chemistry and Chemical Processes, School of Chemistry and Molecular Engineering
East China Normal University
Dongchuan Road 500, Shanghai 200241 (China)
E-mail: ytian@chem.ecnu.edu.cn

Supporting information and the ORCID identification number(s) for the author(s) of this article can be found under: https://doi.org/10.1002/anie.202102833.

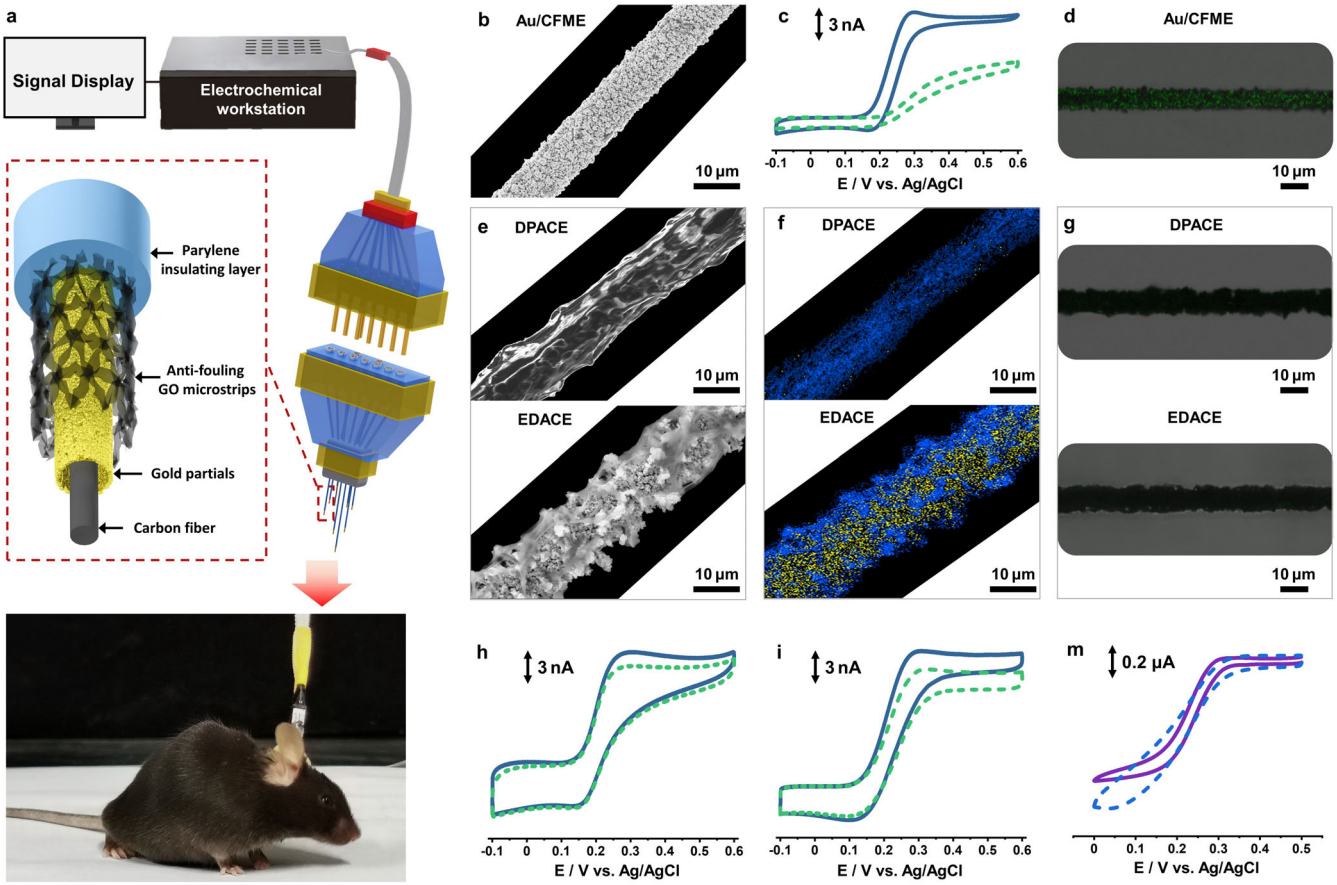

Figure 1. a) Illustration for multi-fiber microarray and measurements in the mouse brain. b) SEM image of Au/CFME. c) Cyclic voltammograms (CVs) obtained at Au/CFME (a) in 10 μM DA solution before (solid curve) and after (dotted curve) the electrode was immersed into 20 mg mL^{-1} FITC-BSA for 2 h. Scan rate: 10 mV s^{-1}. d) Fluorescence image of Au/CFME after immersed in 20 mg mL^{-1} FITC-BSA solution for 2 h. e) SEM images of DPACE (top) and EDACE (bottom). f) EDX analysis of the selected areas of Au (yellow) and GO (blue) on DPACE (top) and EDACE (bottom). g) Fluorescence image of DPACE and EDACE after immersed in 20 mg mL^{-1} FITC-BSA solution for 2 h. h,i) CVs obtained at EDACE (h) and DPACE (i) in 10 μM DA solution before (solid curves) and after (dotted curves) the electrode was immersed into 20 mg mL^{-1} BSA for 2 h. Scan rate: 10 mV s^{-1}. m) CVs obtained at DPACE (solid curve), and EDACE (dotted curve) in 0.5 mM $K_3[Fe(CN)_6]$ with 0.1 M KCl.

of the present microarray with super anti-fouling ability, we found that extracellular concentration of Ca^{2+} was gradually decreased from the superficial to deep brain areas with decreasing rate upon ischemia, then unexpected it recovered from the deep to superficial brain areas with decreasing rate after reperfusion. More interestingly, reduced glutathione (GSH), which can scavenge ROS,[10] effectively reduced Ca^{2+} disorder during I/R processes, suggesting that ROS induced the influx of Ca^{2+} into neurons and resulted in Ca^{2+} overload after ischemia, which was closely related to neuron death. The significant effect of GSH on extracellular Ca^{2+} was also observed during the cerebral hemorrhage model treatment. Therefore, it was suggested that GSH is an essential potential drug for stroke treatment. Moreover, it was discovered that diuretics quickly restored extracellular concentration of Ca^{2+}, but weakened the activity of neurons; while Ca^{2+} blocker–flunarizine restored Ca^{2+} concentration and promoted the neuronal recovery.

Results and Discussion

As a starting point of our work, CFME (ca. 10 μm) with high spatial resolution was prepared, according to our previous methods.[6] Then, gold particles were electrodeposited onto the surface of CFME, which was denoted as Au/CFME electrode. From Figure 1 b, the size of gold particles was estimated to ca. 300–600 nm. According to cyclic voltammetry (CV) (Figure S1a, Supporting Information), the peak current of CFME in 0.1 mM K_3 $[Fe(CN)_6]$ increased by 51 % after gold particles were deposited, demonstrating high electrochemical activity of Au/CFME. But the surface suffers from the adsorption of biological species such as proteins onto the electrode. Because albumin is the most abundant protein in plasma,[11] this kind of natural poison always results in the degraded performance of biosensors for continuous measurements in vivo. As shown in Figures 1 c and d, after the electrode was implanted in bovine serum albumin solution labeled with fluorescein isothiocyanate (FITC-BSA) for 2 h, the signal of Au/CFME in 10 μM dopamine (DA) solution remained only 46.9 % and 84 % of the electrode surface covered by proteins.

Recently, graphene oxide (GO) has attracted much attention because of a random distribution of hydroxyl groups and epoxy groups formed on a single sheet, as well as carboxyl groups and carbonyl groups at the edges of the monolith, which allows GO having super-hydrophilicity with uniform negative charges.[12] On the other hand, most proteins demonstrate negative charge in the neutral solution. Thus, GO was expected to be a potential material for preventing the adsorption of proteins onto electrode surface. Two methods were employed to deposit GO on Au/CFME surface: dip-coating and electrodeposited methods. The developed microelectrodes covered with GOs by these two methods were denoted as DPACE and EDACE, respectively. SEM image (Figure 1e) shows that GO was completely covered the surface of DPACE. However, a portion of gold particles was still exposed on the EDACE surface, while the electrodeposited GOMs were alternately wrapped onto Au/CFME. EDX elemental analysis characterizes elements distribution on the electrode surface (Figure 1f), also demonstrating the interphase exposure of gold and carbon on the EDACE surface. The exposed gold particles on the EDACE surface provided electrochemical active sites for further modification of functionalized molecules.

Next, the anti-fouling effects of EDACE and DPACE were tested in FITC-BSA and solution. From Figure 1g, the surfaces of EDACE with exposed gold particles and DPACE were covered the similar proportion of proteins. However, after the electrode was measured in BSA solution for 2 h, the signal of EDACE in DA solution remained ca. 91.3% (Figure 1h), which was greater than that (Figure 1i) of DPACE (ca. 86.9%). Besides, the oxidation peak showed negligible change for EDACE, but that was obviously shifted 200 mV to positive direction on DPACE. The signals demonstrated negligible changes for EDACE even after immersed in BSA solution upon 60 days. The similar results were also obtained in γ-Globulin solution (Figure S2, Supporting Information). These results proved that EDACE showed better electrochemical performance against protein fouling than DPACE.

Then, CVs of EDACE and DPACE were measured in $K_3[Fe(CN)_6]$ solution (Figure 1m). It was found that EDACE showed more significant signal suppression than DPACE, which may be attributed to more negative charge on EDACE surface than DPACE. Then, Zeta potential was also found to be −18.33 mV on the surface of DPACE, which was higher than that of EDACE, −34.27 mV (Figure S1d, Supporting Information). Most proteins in the brain environment (pH 7.4) were negatively charged, thus EDACE with more negative charge showed repulsive interaction with proteins, resulting in better anti-fouling performance than DPACE. Recent studies have found that the hydrophilic interface was also beneficial for resisting proteins adsorption.[13] Our test showed that the contact angle of Au/GCE modified with electrodeposited GO was $25 \pm 7°$ ($n = 8$, S.D.), which was greater than that of $30 \pm 8°$ ($n = 8$, S.D.) on Au/GCE modified with dip-coated GO (Figure S1g, Supporting Information). Thus, EDACE with electrodeposited GO showed more hydrophilic than DPACE. Therefore, the developed EDACE microelectrode with strong anti-fouling ability was chosen as an optimized electrode surface in the following measurements.

To specifically recognize Ca^{2+} in the brain, three kinds of organic molecules, METH, M18C6, and MBAPTA were designed and synthesized (Figure 2a) as two main parts: recognition groups[14] for selective determination of Ca^{2+} and terminal groups for the molecules self-assembled onto the electrodes. The recognition group of METH shows two pairs of amide bonds in the chain, which could specifically capture Ca^{2+}. M18C6 has an aza crown ether with a cavity size of 260–320 pm to match the size of Ca^{2+}. BAPTA bears four free active carboxyl groups to capture Ca^{2+}. On the other hand, the alkynyl group was designed to stably assemble the molecules onto the electrode surfaces, because Au≡C bond had recently been reported as a robust chemical bond in the brains with abundant thiols.[7] Therefore, all three molecules were characterized by ^{1}H NMR, ^{13}C NMR, and MS (Figures S3–S12, Supporting Information).

Then, the as-prepared EDACE was modified with three kinds of molecules (METH, M18C6, and BAPTA) by Au≡C bond, which were denoted METH-E, M18C6-E, and BAPTA-E (Figure 2a). XPS data demonstrated that all the molecules were stably immobilized onto EDACE surfaces (Figure S14, Supporting Information). Besides, EDACE without modification was employed as an internal reference electrode to provide a built-in correction, thus improving the accuracy of determination in the biological systems. Next, the electrochemical titration of Ca^{2+} was performed using open-circuit potentiometry. The potential of ion-selective electrodes (E_{ISE}) for METH-E, M18C6-E, and BAPTA-E was represented by standard potential E^0, ion concentration term, and potential of reference electrode (E_{RE}). Also, the potential of internal reference electrode (E_{IRE}) was used as a built-in element. Thus, the potential separation ΔE_{ISE} ($\Delta E_{ISE} = E_{ISE} - E_{IRE}$) between E_{ISE} and E_{IRE} was employed for the following titrations.

$$\Delta E_{ISE} = E^0 + \frac{2.303RT}{nF} \lg a_{Ca^{2+}} - E_{RE} - E_{IRE} \quad (1)$$

The ΔE_{ISE} of METH- E, M18C6-E, and BAPTA-E were tested in artificial cerebrospinal fluid (aCSF, 37 °C) with the gradual addition of $CaCl_2$ (Figure 2b). An excellent linear range was observed from 10.0 μM to 31.6 mM for METH-E, while the detection limit was estimated to 5.91 ± 0.33 μM (S/N = 3, $n = 20$, S. D.). For M18C6-E electrode, the linear range was obtained from 3.16 to 3160 μM with a detection limit of 1.89 ± 0.42 μM ($n = 20$, S. D.). Furthermore, the dynamic linearity for MBAPTA-E was obtained in the range of 3.16 to 316 μM, with detection limit down to 0.84 ± 0.32 μM ($n = 20$, S. D.). The sensitivity of MBAPTA-E showed the highest value among those of three kinds of electrode surfaces. However, MBAPTA-E demonstrated a narrow linear range. In contrast, METH-E with a little lower sensitivity exhibited much broader linear range, which matches the concentration range of Ca^{2+} in the brain. The response time of METH- E, M18C6-E, and BAPTA-E was found to less than ca. 1.3 s (Figure S15, Supporting Information), faster than that of commercial glassy ion-selective electrodes (5–15 s). The high

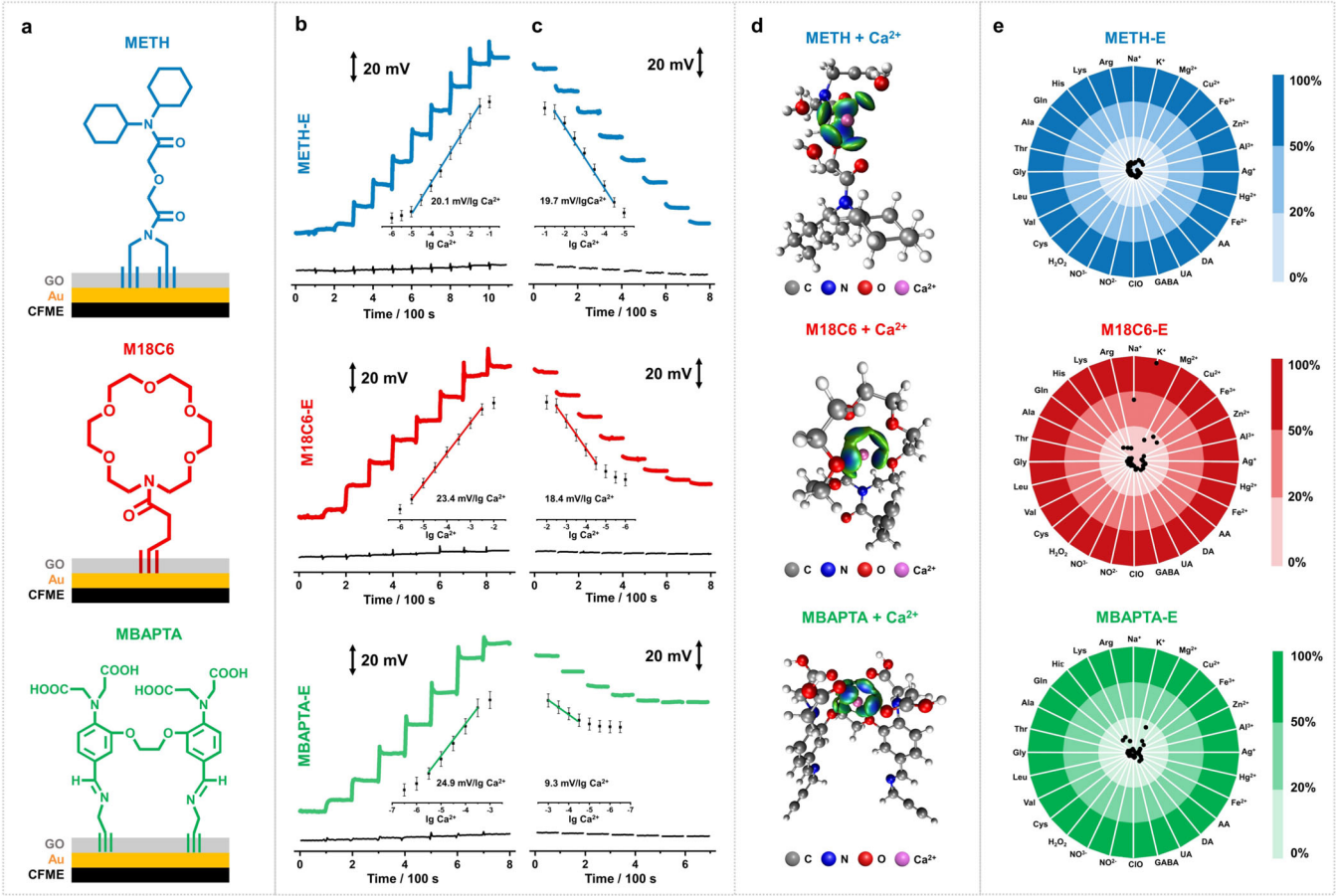

Figure 2. a) Molecular structures of METH (top), M18C6 (middle), and MBAPTA (bottom) and modification of three ligands onto electrode surfaces. b),c) The potential changes (vs. Ag/AgCl) obtained at METH-E (top), M18C6-E (middle), and MBAPTA-E (bottom) with continuously increasing (b) concentration of Ca^{2+} (METH-E was 1 μM–100 mM, M18C6 was 10 μM–10 mM, MBAPTA was 1 μM–1 mM) and decreasing (c) concentration of Ca^{2+} (METH-E was 100 mM–10 μM, M18C6-E was 10 mM–10 μM, MBAPTA-E was 1 mM–0.316 μM) in aCSF without Ca^{2+}. EDACE with unmodified ligand was used as the internal reference electrode (black curve). Inner graphs: Linear fitting plots of potential change versus concentration. d) DFT simulation calculation of the colored isosurface plot of METH (blue), M18C6 (red), and MBAPTA (green) with Ca^{2+}. Blue in isosurface represents electrostatic interaction and green represents dispersion interaction. e) Selectivity test for determination of Ca^{2+} against other metal ions, amino acids, ROS, neuron transmitters obtained at METH-E (top), M18C6-E (middle), and MBAPTA-E (bottom). The concentrations of Ca^{2+} was 100 μM, K^+ and Na^+ were 1 mM, Cu^{2+} and Fe^{3+} were 1 μM, AA was 40 μM, and other species were all 10 μM.

spatial resolution of the developed electrode should be very beneficial for real-time monitoring of Ca^{2+} changes in brain events.

The reversibility of biosensors is also a relatively important feature in establishing real-time tracking methods for quantifying the concentration of Ca^{2+}. The response for METH-E was initially increased with gradual addition of Ca^{2+}, and was reduced with decreasing concentration of Ca^{2+}. The sensitivity of this biosensor was decreased to $98.0 \pm 1.2\,\%$ ($n = 8$, S.D) when the concentration of Ca^{2+} was reduced (Figure 2b). The signal still retained $93 \pm 0.9\,\%$ ($n = 8$, S.D) after 500 increasing and decreasing cycles (Figure S16a, SI). However, for M18C6-E and MBAPTA-E, only $71 \pm 1.3\,\%$ ($n = 8$, S.D) and $29 \pm 0.8\,\%$ ($n = 8$, S.D) of sensitivities were obtained for decreasing cycles compared with those for increasing, which could not satisfy the reversible requirements for in vivo measurements. Moreover, DFT simulation calculations on the binding modes of three ligands for Ca^{2+} (Figure 2d) recognition showed that two carbonyl groups and one ether on METH molecule form a stable complex with $Ca(H_2O)_3^{2+}$, while M18C6 and MBAPTA form complete chelation of Ca^{2+}. The calculation for binding energy (Table S1, Supporting Information) further demonstrated that the binding free energy of METH with Ca^{2+} was significantly smaller than other ligands (Figure 2e). Thus, Ca^{2+} was easy to dissociate at low concentrations, resulting in the advantage of high reversibility.

Next, to investigate whether the binding capacity of the molecules toward Ca^{2+} affects the specific recognition of Ca^{2+} in the complex environments, the selectivity for three electrodes was tested for determination of Ca^{2+}over other metal ions, amino acids, ROS, neurotransmitters, and so on (Figure 2c; Figure S17, Supporting Information). Obviously, M18C6-E was easily affected by K^+ (ca. 91 %), Na^+ (ca. 45 %), and Cu^{2+} (ca. 18 %). This observation may be due that the M18C6 ligand traps ions because of matching the size of its cavity. Thus, the ions with similar sizes to the cavity show comparable responses with Ca^{2+}, which made it difficult to

separate the responses of K^+ and Na^+ from that of Ca^{2+}. The main interference obtained at MBAPTA-E against the determination of Ca^{2+} was found to be Mg^{2+} (ca. 16%) because the structure of 4 carboxyl groups could also be easy to form a chelate with Mg^{2+}. Fortunately, METH-E demonstrated no detectable interferent (< ca. 3.0%). Due to the special molecular structure with two amide groups, METH-E has a particularly capture capacity for Ca^{2+}. After a comprehensive comparison for the three kinds of electrodes from dynamic linear range, sensitivity, reversibility, and selectivity, METH-E was chosen as the optimized biosensor because of its superior reversibility and selectivity, suitable detection range, and acceptable sensitivity. Next, to test the anti-fouling ability of METH-E, it was implanted in the mouse brain for 60 days. It was found that the sensitivity of this electrode still maintained $92 \pm 0.6\%$ ($n = 8$, S.D; Figure S16b, Supporting Information), compared with that of the control experiment, proving that METH-E could work steadily for a long period up to 2 months in a biological environment such as brain. Finally, the biological damage of METH-E was characterized by TTC staining experiments (Figure S16c, Supporting Information). We found that the mouse brain remained intact activity after stained with TTC after the microfiber electrode was implanted into the mouse brain for 60 days, demonstrating that our developed microelectrode had quite low damage and was competent for subsequent in vivo experiments.

As demonstrated above, the developed METH-E showing high selectivity and reversibility for Ca^{2+} recognition with excellent biocontamination resistance established a reliable and durable approach for real-time tracking and continuously monitoring the levels of Ca^{2+} in the live brain. Then, 7 METH-E electrodes with different lengths and internal reference electrode were constructed into a microelectrode array (Figure 3a,b) with the same active tip length of 300 μm, which made it possible to simultaneously monitor the concentration of Ca^{2+} in the brain regions with different depths in the same mouse. Meanwhile, the electrophysiological electrode was also integrated with the array to record LFP signals. Next, the developed METH-E microarray was implanted into 7 regions of the mouse brain (Figure 3b), such as the primary motor cortex (M1), primary somatosensory barrel) cortex (S1BF), hippocampal CA1 (CA1) hippocampal dentate gyrus (DG), lateral dorsal (LD), caudate-putamen (CPu), and reticular nuclei (RT). It was the first observation that the initial change time and decreasing rate of Ca^{2+} in each brain area were different upon ischemia (Figure 3d). Simultaneous measurements of LFP (Figure 3f) during ischemia showed a large suppression of discharge, proving the ischemic state of neurons. Specifically, the extracellular $[Ca^{2+}]$ changed at ca. 1.11–1.24 min in the superficial cortical areas (M1, S1BF) and then at ca. 2.44–2.71 min in the hippocampus (CA1, DG) after ischemia, while the changes in the deep areas (LD, CPu, RT) response was much later after ca. 4.44–4.75 min. Meanwhile, the decreasing rate of $[Ca^{2+}]$ in superficial brain areas (M1, S1BF, CA1, DG) was 0.25–0.31 mM min^{-1}, which was faster than that of 0.10–0.11 mM min^{-1} in deep brain areas (LD, CPu, RT Figure 3d). At the end of ischemia for 20 min, the extracellular $[Ca^{2+}]$ was finally decreased to 0.15–0.21 mM in superficial brain regions (M1, S1BF, CA1, DG), much lower than that of 0.43–0.63 mM in deep brain regions (LD, CPu, RT). These data indicated that the sensitivity of each brain area toward ischemia was different. Since the blood vessel density in the superficial brain area was lower than that in the deep layer, it was reasonable that hypoxia and Ca^{2+} influx firstly occur in the superficial layer. Then, the duration of ischemia was extended to 45 and 90 min. It was observed that extracellular $[Ca^{2+}]$ was decreased to 50–60% and further to 27–45% (vs. 20 min ischemia) at the end of ischemia for 45 and 90 min, respectively. These in vivo data indicated that the decrease in extracellular $[Ca^{2+}]$ became more severe with the prolonged ischemia time. The above data were collected by the same microarray after implanted for 5 days (Figure 3c).

Next, the arterial embolism was removed for reperfusion using the same electrode. Benefiting from the high reversibility of METH-E microarray, the fluctuation of Ca^{2+} concentration was accurately and continuously monitored. Specifically, taking 20 min I/R as an example, the extracellular $[Ca^{2+}]$ in deep brain regions of LD, CPu and RT was recovered after ca. 0.71–0.79 min of reperfusion (Figure 4d), and increased to ca. 97% of the baseline value. While in the superficial brain regions of M1, S1BF, CA1, and DG it was slowly recovered after ca. 3.05–3.25 min of reperfusion and eventually reached ca. 92% of the baseline value. For reperfusion after 45- and 90-min ischemia, the extracellular $[Ca^{2+}]$ of each brain area was still recovered more than 70% of the initial value. Since the middle artery was located closer to the deep brain area, $[Ca^{2+}]$ was recovered first. It was worth noting that TTC staining of mice brain slices after 20 min I/R showed that the infarct area was less than ca. 2% (Figure 3e), proving the good activity of each brain area. When the ischemia time was further extended to 45 and 90 min, despite Ca^{2+} recovery was > 83% after reperfusion, a large area of infarction (> 35%) was observed in TTC staining experiments (Figure 3e). The LFP signal after reperfusion further proved that neuronal discharge was hardly recovered after prolonged ischemia. Our previous research had shown that more ROS was produced after reperfusion.[15] Ca^{2+} was transferred into cells upon ischemia, which generated a large amount of ROS in mitochondria.[16] Although, as shown above, extracellular Ca^{2+} was almost recovered after reperfusion, the produced ROS in live cells changed the intracellular ATP content, which eventually led to mitochondrial Ca^{2+} overload and neurons death.[17]

To further analyze the relationship between ROS and Ca^{2+} overload and neuronal death, GSH, the scavenger of ROS, was injected into the mice with 400 and 800 mg kg^{-1} before MCAO surgery. In the 400 mg kg^{-1} mice group upon ischemia for 20, 45, and 90 min, the decreasing rate of $[Ca^{2+}]$ was effectively reduced to 53–71% of the control group in M1, S1BF, CA1, DG, LD, CPu, and RT areas. Moreover, GSH also significantly increased the recovery rate of extracellular Ca^{2+} during reperfusion after ischemia (Figure 3d). After 20, 45, and 90 I/R, the $[Ca^{2+}]$ recovery rate of each brain area was increased to 132–145%, 156–168%, and 185–193% of the control group, respectively. The subsequent TTC staining experiments showed that after ischemia for 90 min, the infarction area (Figure 3e) for 400 mg kg^{-1} GSH administra-

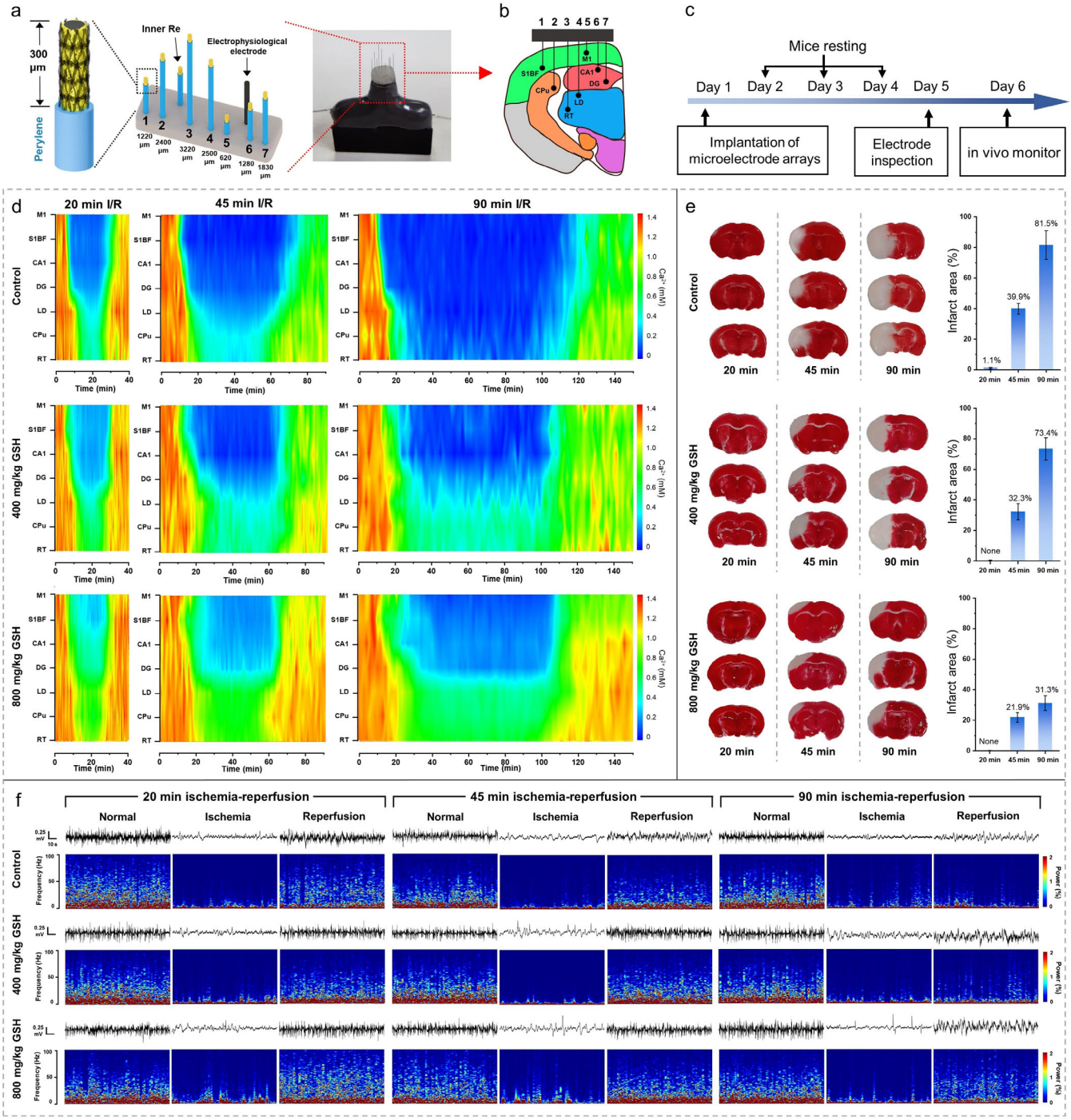

Figure 3. a) Photograph and diagram of the METH-E microarray. The active tip of each electrode was exposed to 300 μm, and the rest was evenly covered with parylene insulating layer. Both internal reference (Inner Re) and electrophysiological electrodes were integrated with microelectrode array. b) METH-E multi-fiber array inserted into 7 brain regions (M1, S1BF, CA1 DG, LD, CPu, and RT). Black spot represents the position that an electrode implanted. c) Flow chart of in vivo monitoring of I/R processes. d) Heat maps for extracellular [Ca^{2+}] changes obtained at METH-E microarray in 7 brain regions for 20 min (left), 45 min (middle), and 90 min (right) upon ischemia and then reperfusion. e) TTC-stained brain tissues and statistics of infarct areas after 20, 45, and 90 min I/R ($n = 8$, S. D.). f) Local field potential (LFP) curves and power spectra obtained at METH-E microarray in hippocampus CA1 for 20 min (left), 45 min (middle), and 90 min (right) upon I/R processes.

tion group was $73.4 \pm 7.4\,\%$ ($n = 8$, S.D., the same below for in vivo experiments), which was smaller than that of the control group ($81.5 \pm 9.3\,\%$, Figure 3d). With an increasing dose of GSH to 800 mg kg^{-1}, the decreasing rate of Ca^{2+} after cerebral ischemia in the brain was reduced to 34–45 %, and the recovery rate of Ca^{2+} after reperfusion was increased to 214–240 %. Even after ischemia for 90 min, the area of cerebral infarction in the 800 mg kg^{-1} GSH administration group was only $31.3 \pm 4.9\,\%$. Meanwhile, the LFP signal also confirmed that the discharge energy of neurons after reperfusion

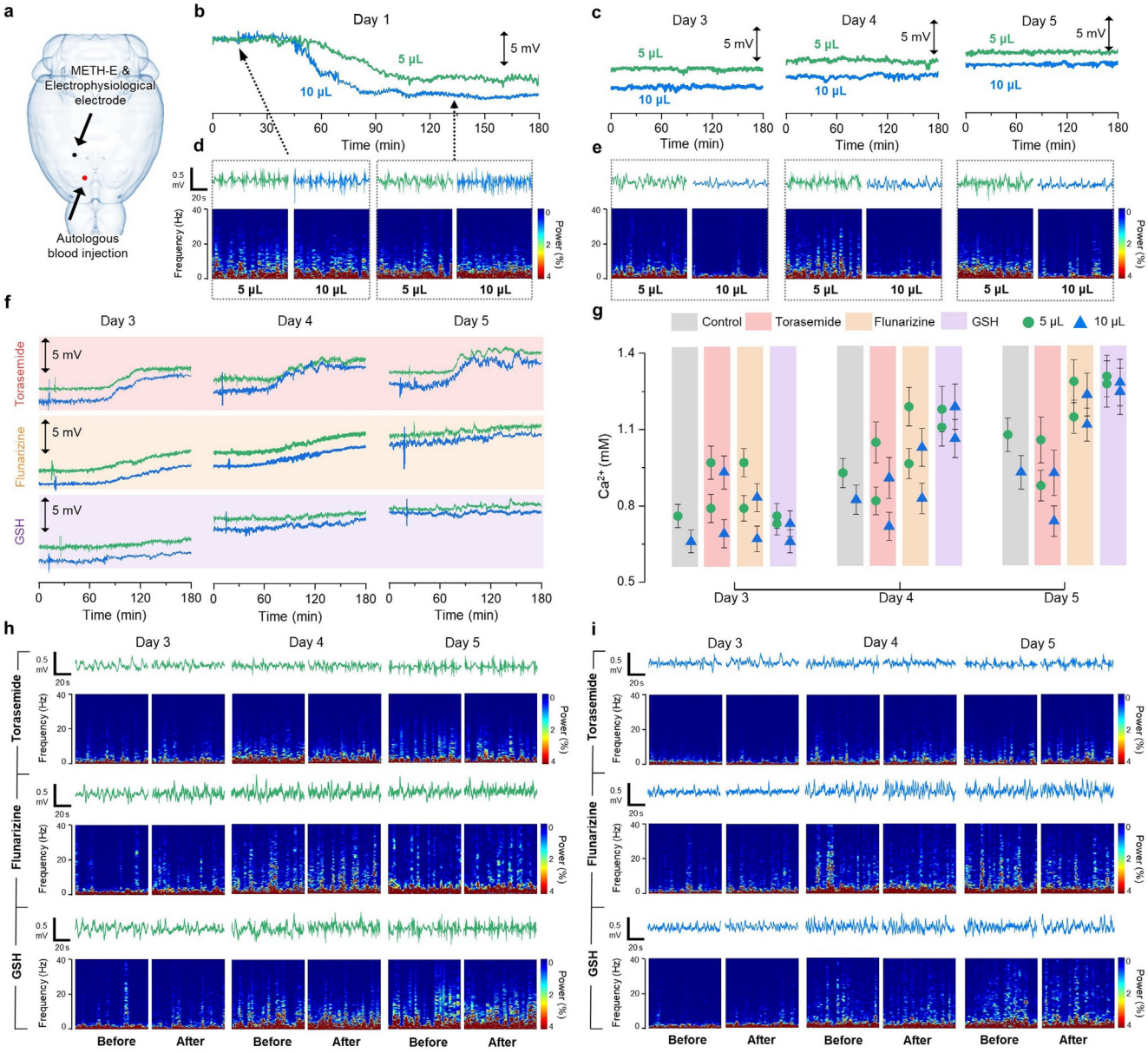

Figure 4. a) Diagram of METH-E and electrophysiological electrode implantation location and autologous blood injection location. b),c) Extracellular [Ca^{2+}] changes obtained from the 5 μL group (green curve) and 10 μL group (blue curve) in CA1 area when autologous blood was injected into the mouse caudate nucleus (Day 1) and the control group of subsequent 3–5 days recovery period. d),e) Local field potential (LFP) obtained from the 5 μL group (green curves) and 10 μL group (blue curves) in CA1 area of mice in the control group at Day 1 (d) and Day 3–5 (e). f)–i) Potentiometric curves recorded at METH-E in the hippocampus of mice (f), statistics ($n = 8$, S.D.) of extracellular [Ca^{2+}] changes (g), and local field potential curves with power spectra (h,i) obtained from the 5 μL group (h) and 10 μL group (i) in CA1 area upon the treatment of torasemide, flunarizine, and GSH.

recovered more significantly with increasing dose of GSH (Figure 3d), which was the direct evidence of the restoration of neuronal vitality. In summary, it was found for the first time that GSH effectively reduced Ca^{2+} disorder during I/R and further protected the neuronal activity. Previous reports have suggested that initial Ca^{2+} influx through glutamate receptors after ischemia.[18] Our results suggested that the generated ROS upon ischemia and reperfusion may be one of the critical factors for the massive influx of extracellular Ca^{2+}, which eventually resulted in neuron death after I/R processes.

Cerebral hemorrhage is a common subtype of stroke. It often occurs in the basal ganglia and further affects the hippocampus.[19] Therefore, the developed microelectrode was adjusted to continuously monitor extracellular [Ca^{2+}] in the hippocampus of mice after basal ganglia hemorrhage. To simulate different degrees of spontaneous intracerebral hemorrhage (SICH), two doses of autologous blood (5 and 10 μL) were injected into the striatum of mice brain (Figure 4a), which were denoted as the 5 μL and 10 μL groups, respectively. The concentration of Ca^{2+} in CA1 area was

gradually decreased from initial 1.30 ± 0.15 mM to 0.63 ± 0.12 mM and 0.55 ± 0.11 mM for the 5 μL and 10 μL groups, respectively (Figure 4b).

Then, after the model mice rest for 2 days, we monitored the effects of two drugs of torasemide and flunarizine on extracellular Ca^{2+} and LFP signals during SICH treatment for 3 days. On the first day after the torasemide was delivered, the concentrations of Ca^{2+} in CA1 area for the 5 μL and 10 μL groups were increased to 0.94 ± 0.19 mM and 0.85 ± 0.18 mM, respectively (Figure 4f), compared to 0.65 ± 0.13 mM and 0.56 ± 0.11 mM of the control groups with self-recovery (Figure 4c). However, after the treatment on Day 3, the concentrations of Ca^{2+} in the 5 μL group and 10 μL group were not restored to more than ca. 1.1 mM yet. Moreover, the discharge of LFP was also inhibited in the consecutive treatment of 3 days, and even worse than the control group (Figure 4h,i). The results indicated that although the diuretic torsemide restored the concentration of Ca^{2+}, the neuronal firing activity was not improved, possibly due that the dehydrating drug torasemide just relaxes blood vessels[20] and speeds up metabolism. Next, with the treatment of another drug, flunarizine, the concentrations of Ca^{2+} were slowly increased in CA1 area of the 5 μL and 10 μL groups to 0.76 ± 0.15 mM and 0.71 ± 0.14 mM, respectively, on the first day. More interestingly, the concentrations of extracellular Ca^{2+} were significantly restored to 1.27 ± 0.16 mM and 1.22 ± 0.14 mM, respectively on Day 3 of treatment (Figure 4f,g). Meanwhile, the LFP signal almost returned to the basal line on Day 3. The data showed that flunarizine not only blocked the excessive influx of Ca^{2+},[21] but also improved the balance of Ca^{2+} in neuronal activity.

We have demonstrated the essential regulatory effect of ROS on Ca^{2+} above. Thus, we then studied the impact of GSH treatment on Ca^{2+} and LFP after cerebral hemorrhage. After continuous treatment of 50 mg kg^{-1} GSH, the concentrations of Ca^{2+} in CA1 area recovered slightly to 0.69 ± 0.12 mM and 0.62 ± 0.11 mM of the 5 μL and 10 μL groups on the first day, respectively (Figure 4f,g). Subsequently, they finally recovered to 1.18 ± 0.16 mM and 1.10 ± 0.18 mM on Day 3. Also, the discharge state of LFP was significantly restored compared to the control groups (Figure 4h,i). The results suggested that the scavenger of ROS, GSH, can also play as a potential drug for treating cerebral hemorrhage. According to the above results, we believed that SICH patients should not only pay attention to intracranial pressure[22] during drug treatment but also the changes in Ca^{2+} for protection of brain activity. This high-performance multi-fiber microarray established a reliable approach for in vivo screening drugs and pharmacological research.

Conclusion

We have developed an anti-biological fouling multi-fiber microarray for real-time monitoring of reversible changes of extracellular Ca^{2+} and neuron activity in many regions of the brain in both head-fixed and freely moving mice. The sensitivity of this microfiber array has remained ca. 92% responses of Ca^{2+} after continuous measurements in the live brain for 60 days. On the other hand, three kinds of molecules with different affinities toward Ca^{2+} have been designed and synthesized for selective and reversible recognition of Ca^{2+}. It has been found that the low binding strength of Ca^{2+} ligand–METH is beneficial for the reversible capture and dissociation when Ca^{2+} concentration fluctuates. Fortunately, it is worth noting that METH still demonstrates high selectivity for determination of Ca^{2+} against other metal ions, ROS, amino acids. This is the first report that the developed microelectrode array has demonstrated both remarkable reversibility and good selectivity, which can be used to continuously monitor the levels of Ca^{2+} for 60 days in the live brain without negligible signals loss. Using this powerful tool, we have firstly found that extracellular concentration of Ca^{2+} is gradually decreased with decreasing rate from superficial to deep brain areas during ischemia, and progressively recovered with deceleration rate from deep to superficial brain areas after reperfusion. This indicates that our microarray has provided a useful and powerful tool for investigating complex pathological processes involved large-scale network dynamics across multiple brain regions. Moreover, it has been discovered the influx of Ca^{2+} is more effectively reduced as the dose of GSH, a scavenger of ROS, is increased. Thus, GSH can be used as an effective inhibitor to protect neuron activities. Finally, it has been found that the Ca^{2+} channel blocker (flunarizine) not only gradually restores the concentration of Ca^{2+} in the treatment of cerebral hemorrhage but also promotes the recovery of neurons. This further confirms the direct connection between Ca^{2+} influx and cerebral hemorrhage injury.

The number of electrodes in the array can be further increased in the future and eventually realize large-scale dynamically recording of neuronal signaling with chemical expression across the whole brain. Also, the developed multi-fiber microelectrode array can be combined with photometry to simultaneously monitor intracellular and extracellular chemical signals in the live brain of both head-fixed and freely moving animals for understanding the physiological and pathological processes and screening the drugs. Therefore, our work has opened up a new way to studying the neurons in the whole brain through real-time tracking and accurate quantifying of the concentrations, distributions, and changing speeds of chemical species in the brain. Moreover, we have provided a methodology to construct long-range stable, reversible, and selective molecular probes suitable for investigating brain signals. These methods should bring new insights for understanding the brain events, as well as for treating brain diseases and developing artificial brains.

Acknowledgements

This work was supported by NSFC (Nos. 21635003 and 21811540027) and Innovation Program of Shanghai Municipal Education Commission (No. 201701070005E00020).

Conflict of interest

The authors declare no conflict of interest.

Keywords: anti-biofouling · brain · microfiber arrays · reversibility · stroke

[1] J. Blagg, P. Workman, *Cancer Cell* **2017**, *32*, 9 – 25.

[2] a) J. Abbott, T. Ye, D. Ham, H. Park, *Acc. Chem. Res.* **2018**, *51*, 600 – 608; b) D. Gonzales, K. Badhiwala, D. Vercosa, B. Avants, Z. Liu, W. Zhong, J. Robinson, *Nat. Nanotechnol.* **2017**, *12*, 684 – 691.

[3] a) T. Lee, L. Cai, V. Lelyveld, A. Hai, A. Jasanoff, *Science* **2014**, *344*, 533 – 535; b) Z. Zhou, L. Yang, J. Gao, X. Chen, *Adv. Mater.* **2019**, *31*, 1804567.

[4] a) X. Wu, Y. Zhao, J. Ding, Z. Si, D. Cheng, H. Shi, X. Wang, *Epilepsia* **2018**, *59*, 1655 – 1666; b) A. Miranda, G. Dorien, D. Bertoglio, J. Vleugels, G. Bruyne, S. Stroobants, S. Staelens, J. Verhaeghe, *J. Nucl. Med.* **2019**, *60*, 844 – 850.

[5] a) C. Amatore, Y. Bouret, E. Travis, R. Wightman, *Angew. Chem. Int. Ed.* **2000**, *39*, 1952 – 1955; *Angew. Chem.* **2000**, *112*, 2028 – 2031; b) W. Zhu, C. Gu, J. Dunevall, L. Ren, X. Zhou, A. Ewing, *Angew. Chem. Int. Ed.* **2019**, *58*, 4238 – 4242; *Angew. Chem.* **2019**, *131*, 4282 – 4286; c) Y. Liu, W. Huang, *Angew. Chem. Int. Ed.* **2021**, *60*, 2757 – 2767; *Angew. Chem.* **2021**, *133*, 2789 – 2799.

[6] a) M. Zhuang, C. Ding, A. Zhu, Y. Tian, *Anal. Chem.* **2014**, *86*, 1829 – 1836; b) Y. Luo, L. Zhang, W. Liu, Y. Yu, Y. Tian, *Angew. Chem. Int. Ed.* **2015**, *54*, 14053 – 14056; *Angew. Chem.* **2015**, *127*, 14259 – 14262; c) L. Liu, F. Zhao, W. Liu, T. Zhu, J. Z. H. Zhang, C. Chen, Z. Dai, H. Peng, J. L. Huang, Q. Hu, W. Bu, Y. Tian, *Angew. Chem. Int. Ed.* **2017**, *56*, 10471 – 10475; *Angew. Chem.* **2017**, *129*, 10607 – 10611; d) W. Liu, H. Dong, L. Zhang, Y. Tian, *Angew. Chem. Int. Ed.* **2017**, *56*, 16328 – 16332; *Angew. Chem.* **2017**, *129*, 16546 – 16550; e) H. Dong, Q. Zhou, L. Zhang, Y. Tian, *Angew. Chem. Int. Ed.* **2019**, *58*, 13948 – 13953; *Angew. Chem.* **2019**, *131*, 14086 – 14091.

[7] C. Zhang, Z. Liu, L. Zhang, A. Zhu, F. Liao, J. Wan, J. Zhou, Y. Tian, *Angew. Chem. Int. Ed.* **2020**, *59*, 20499 – 20507; *Angew. Chem.* **2020**, *132*, 20680 – 20688.

[8] S. Moulton, J. Barisci, A. Bath, R. Stella, G. Wallace, *J. Colloid Interface Sci.* **2003**, *261*, 312 – 319.

[9] a) L. Mao, J. Jin, L. Song, K. Yamamoto, L. Jin, *Electroanalysis* **1999**, *11*, 499 – 504; b) Y. Singh, L. Sawarynski, P. Dabiri, W. Choi, A. Andrews, *Anal. Chem.* **2011**, *83*, 6658 – 6666; c) X. Liu, T. Xiao, F. Wu, M. Shen, M. Zhang, H. Yu, L. Mao, *Angew. Chem. Int. Ed.* **2017**, *56*, 11802 – 11806; *Angew. Chem.* **2017**, *129*, 11964 – 11968.

[10] U. Förstermann, *Nat. Clin. Pract. Card.* **2008**, *5*, 338 – 349.

[11] Z. Liu, X. Chen, *Chem. Soc. Rev.* **2016**, *45*, 32 – 56.

[12] a) J. Kim, L. Cote, J. Huang, *Acc. Chem. Res.* **2012**, *45*, 1356 – 1364; b) V. Palermo, L. Kinloch, S. Ligi, N. Pugno, *Adv. Mater.* **2016**, *28*, 6232 – 6238.

[13] Q. Wei, T. Becherer, S. Angioletti-Uberti, J. Dzubiella, C. Wischke, A. Neffe, A. Lendlein, M. Ballauff, R. Haag, *Angew. Chem. Int. Ed.* **2014**, *53*, 8004 – 8031; *Angew. Chem.* **2014**, *126*, 8138 – 8169.

[14] a) W. Wang, W. Erdahl, S. Hamidinia, C. Chapman, D. Pfeiffer, *Biophys. J.* **2001**, *81*, 3275 – 3284; b) R. Izatt, K. Pawlak, J. Bradshaw, *Chem. Rev.* **1991**, *91*, 1721 – 2085; c) T. John, P. Singh, A. Levy, R. London, *J. Inorg. Biochem.* **1987**, *31*, 113 – 121.

[15] Z. Wang, D. Liu, H. Gu, A. Zhu, Y. Tian, G. Shi, *Biosens. Bioelectron.* **2013**, *43*, 101 – 107.

[16] P. Hernansanz-Agustín, C. Choya-Foces, S. Carregal-Romero, E. Ramos, T. Oliva, T. Villa-Piña, L. Moreno, A. Izquierdo-Álvarez, J. Cabrera-García, A. Cortés, A. Lechuga-Vieco, P. Jadiya, E. Navarro, E. Parada, A. Palomino-Antolín, D. Tello, R. Acín-Pérez, J. Rodríguez-Aguilera, P. Navas, A. Cogolludo, I. López-Montero, A. Martínez-Del-Pozo, J. Egea, M. López, J. Elrod, J. Ruíz-Cabello, A. Bogdanova, J. Enríquez, A. Martínez-Ruiz, *Nature* **2020**, *586*, 287 – 291.

[17] a) Z. Wu, M. Liu, Z. Liu, Y. Tian, *J. Am. Chem. Soc.* **2020**, *142*, 7532 – 7541; b) Z. Liu, H. Pei, L. Zhang, Y. Tian, *ACS Nano* **2018**, *12*, 12357 – 12368.

[18] D. Bano, K. Young, C. Guerin, R. LeFeuvre, N. Rothwell, L. Naldini, R. Rizzuto, E. Carafoli, P. Nicotera, *Cell* **2005**, *120*, 275 – 285.

[19] a) Y. Yakushiji, D. Werring, *Nat. Rev. Neurol.* **2016**, *12*, 680 – 682; b) Q. Chen, J. Zhang, J. Guo, J. Tang, Y. Tao, L. Li, H. Feng, Z. Chen, *Transl. Stroke Res.* **2015**, *6*, 125 – 132.

[20] A. Fortuño, P. Muñiz, S. Ravassa, G. Zalba, M. Fortuño, J. Díez, *Hypertension* **1999**, *34*, 138 – 143.

[21] a) M. Vos, A. Gorgels, J. Leunissen, H. Wellens, *Circulation* **1990**, *81*, 343 – 349; b) T. Kuga, J. Sadoshima, H. Tomoike, N. Akaike, M. Nakamura, *Circ. Res.* **1990**, *67*, 469 – 480.

[22] R. Macdonald, *Nat. Rev. Neurol.* **2014**, *10*, 44 – 58.

Manuscript received: February 24, 2021
Accepted manuscript online: April 1, 2021
Version of record online: ■■ ■■, ■■■■

Research Articles

Microfiber Arrays

Y. Liu, Z. Liu, F. Zhao,
Y. Tian* ———— ▮▮▮▮–▮▮▮▮

Long-Term Tracking and Dynamically Quantifying of Reversible Changes of Extracellular Ca^{2+} in Multiple Brain Regions of Freely Moving Animals

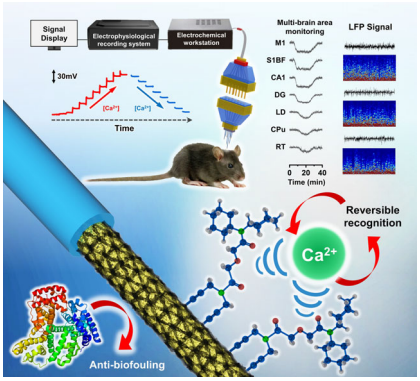

An anti-biofouling microfiber array was created to real-time tracking and reversibly quantifying of extracellular concentration of Ca^{2+} together with neuron activity across many regions in freely moving mammalian brain for 60 days. The changing sequence and rate of Ca^{2+} in 7 brain regions were different during the stroke, and ROS scavenger could protect Ca^{2+} influx and neuronal activity after stroke.